ACS APPLIED MATERIALS & INTERFACES

Research Article

www.acsami.org

Coaxially Electrospun Axon-Mimicking Fibers for Diffusion Magnetic Resonance Imaging

Feng-Lei Zhou,[†,‡] Penny L. Hubbard,[†,§] Stephen J. Eichhorn,[∥] and Geoffrey J.M. Parker*[,†,§]

[†]Centre for Imaging Sciences, Manchester Academic Health Science Centre, [§]Biomedical Imaging Institute, and [‡]Materials Science Centre, School of Materials, The University of Manchester, Manchester M13 9PT, United Kingdom

[∥]Physics, College of Engineering, Mathematics and Physical Sciences, University of Exeter, Exeter EX4 4QF, United Kingdom

ABSTRACT: The study of brain structure and connectivity using diffusion magnetic resonance imaging (dMRI) has recently gained substantial interest. However, the use of dMRI still faces major challenges because of the lack of standard materials for validation. The present work reports on brain tissue-mimetic materials composed of hollow microfibers for application as a standard material in dMRI. These hollow fibers were fabricated via a simple and one-step coaxial electrospining (co-ES) process. Poly(ε-caprolactone) (PCL) and polyethylene oxide (PEO) were employed as shell and core materials, respectively, to achieve the most stable co-ES process. These co-ES hollow PCL fibers have different inner diameters, which mainly depend on the flow rate of the core solution and have the potential to cover the size range of the brain tissue we aimed to mimic. Co-ES aligned hollow PCL fibers were characterized using optical and electron microscopy and tested as brain white matter mimics on a high-field magnetic resonance imaging (MRI) scanner. To the best of our knowledge, this is the first time that co-ES hollow fibers have been successfully used as a tissue mimic or phantom in diffusion MRI. The results of the present study provide evidence that this phantom can mimic the dMRI behavior of cellular barriers imposed by axonal cell membranes and myelin; the measured diffusivity is compatible with that of in vivo biological tissues. Together these results suggest the potential use of co-ES hollow microfibers as tissue-mimicking phantoms in the field of medical imaging.

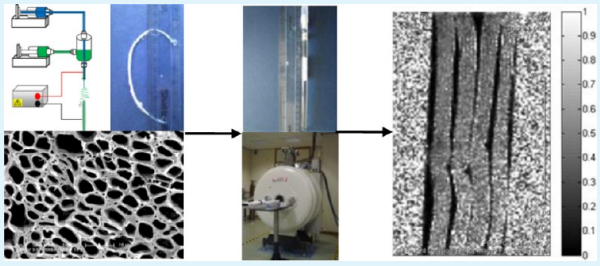

KEYWORDS: *coaxial electrospinning, hollow fibers, diffusion magnetic resonance imaging, phantom*

INTRODUCTION

Brain structure and internal connectivity are areas of substantial past and current research activity. Diffusion magnetic resonance imaging (dMRI) provides a noninvasive tool to explore brain tissue by the measurements of the passive diffusion of tissue water among the cellular structures, the classic example being the anisotropic diffusion observed within white matter.[1] Brain white matter consists of highly ordered bundles at the molecular (filaments), microscopic (axons), and macroscopic (tracts) length scales, with orientationally coherent structure often persisting for more than the MRI voxel length scale (~2 mm). This tissue, with its highly organized hierarchical structures, leads to an orientationally anisotropic fibrous arrangement in vivo, both in animals and in humans.

MRI tissue mimics or phantoms for neurological use have to date proved to be a promising, but limited, tool for calibration and validation of dMRI methods, such as tractography and microstructure measurement.[2,3] These phantoms aim to approximate the cellular structure of tissues (micrometers) and the long-range connections within the brain (centimeters). It is advantageous to have a phantom that exhibits the same or similar properties ("cell" size, "tract" structure, "membrane" permeability, etc.) to human and/or animal tissue, but there are significant problems with using the existing phantoms for brain dMRI.[4]

Examples of existing phantom materials are natural plant materials (e.g., asparagus stems), animal tissues, (e.g., excised pig and rat spinal cord) as well as other animal nerve structures (e.g., garfish or lobster nerves), all of which have been used as biological phantoms.[5−9] The exact microstructure and diffusion characteristics of these materials are however generally not a close match to in vivo human tissue, and they are inherently uncontrollable in experimental use and change on excision and preservation and during storage. They are therefore poor choices for calibration purposes, although an MRI compatible viable isolated tissue maintenance chamber, which allows white matter tissue to be kept in a viable in vivo state for many hours, could enable animal tissues to perform better as phantoms.[10] Synthetic phantoms, which aim to mimic axons and fiber bundles, such as those made from glass or plastic capillary and textile filament fibers, have been proposed to overcome these issues.[9,11−14] However, the rigidity of glass capillaries and the large diameters of plastic capillaries impose limits to the macroscopic and microscopic geometry of phantom design. None of the available textile filament fibers are hollow, and all existing synthetic options have very low and fixed membrane

Received: September 7, 2012
Accepted: November 7, 2012
Published: November 7, 2012

   dx.doi.org/10.1021/am301919s | ACS Appl. Mater. Interfaces 2012, 4, 6311−6316

permeability. It is also challenging to regulate the angular distribution of fibers and construct complex fiber geometries such as crossing, kissing or branching present in human brain tissue. As a result, the dissimilarity between the microscopic geometry of the existing phantoms and that of brain tissue sets a limit on the degree of validation that they can provide and, to date, has necessitated the use of live animal studies in which the measured diffusion characteristics can be validated against tract tracer methods and post-mortem histology.[4]

Diffusion MRI is a commonly used tool in clinical and research MRI centers worldwide. However, the quantitative use of dMRI and comparisons between centers is hindered by scanner-specific hardware performance variations and scanner calibration variations. There is therefore a need for the development of robust, stable, and realistic calibration objects that can be used for standardization purposes. The above considerations motivate the search for fiber phantoms with a well-defined structure, composition and architectural organization.

There have been only a few studies that have used hollow fibers for constructing dMRI phantoms for the validation and calibration of magnetic resonance methods.[15−17] However, these studies usually made use of commercial hollow fiber modules, i.e., dialyzer and bioreactors, which are not specially fabricated for dMRI applications. Additionally, their inner diameters are far too large, typically 200−300 μm, compared with those of tissue cell structure, where for example, axon fibers range in diameters from 0.1−10 μm, and cardiac muscle fibers have ∼15 μm diameters.[18,19] There is no single available solution to the challenge of converting available glass/plastic capillary or textile filament fibers into truly biomimetic phantoms in dMRI.

No previous studies have been carried out which employ electrospun hollow fibers to mimic tissues, such as brain and cardiac muscle, although there have been extensive reports on the use of electrospun solid fibers as extracellular matrix (ECM)-mimetic materials in tissue engineering.[20,21] We have recently shown that coaxial electrospinning (co-ES) could offer an alternative solution to this challenge, since it is possible to produce controllable hollow polymer microfibers − the first building elements in the creation of white-matter mimicking phantoms.[22] There have not been previous reports of any approach that has the flexibility and realistic manufacturing route of this method, particularly for matching structures both at microscopic and macroscopic levels. However, there are challenges facing co-ES to produce practical and realistic phantoms composed of hollow microfibers with appropriate thickness to be used with the typical spatial resolution attainable with MR scanners. It is widely accepted that the productivity of the single needle electrospinning process is typically less than 1.0 g h^{-1} by fiber weight.[23] For instance, electrospun fiber webs have the thickness of ∼0.02 mm for typical application in protective textiles and tissue engineering.[24,25] In the case of Co-ES, hollow fibers themselves have a small diameter, and the thickness of the resultant fiber assemblies can likewise be quite small. The production of thicker co-ES fiber samples requires longer operation time for the electrospinning process. The longer operation time can in turn lead to challenges for process stability, which is required in order to maintain the sample quality through the thickness of the sample.

The present work aims to produce hollow microfibers with similar sizes those seen in brain white matter and with an appropriate sample thickness via a one-step co-ES technique with the final purpose of providing novel tissue mimetic materials with which to validate new and existing MRI methodology and to provide calibration objects for MRI scanners. Importantly, such materials will help alleviate the need to perform animal studies and minimize the use of human/animal sample or in vivo studies.

EXPERIMENTAL SECTION

Materials. Polyethylene oxide (PEO) has been chosen to replace the sugar aqueous solution used in our previous study as a core material.[22] PEO is electrospinnable, thus allowing a stable coaxial electrospinning process to be achieved over a wide range of process parameters. Additionally, the resultant polycaprolactone (PCL) hollow fibers have average inner diameters closer to the size of the axons we wish to mimick, compared to those obtained in our previously prepared sugar−PCL core−shell fiber bundles. PCL (weight average molecular weight M_w = 70 000−90 000) and PEO (viscosity average molecular weight M_v = 900 000) were obtained from Sigma Aldrich (Dorset, UK) and used as received. The solvents chloroform, N,N-dimethyl-formamide (DMF) and cyclohexane were also purchased from Sigma Aldrich (Dorset, UK). Deionized water was used to dissolve the PEO.

Co-ES. Core/shell fibers were fabricated by a co-ES process using the setup described by Zhou et al.[22] All experiments were conducted in a fume cupboard at ambient conditions. In a typical procedure for co-ES, a 10 w/w% solution of PCL in chloroform/DMF (8:2, w/w) was used as the shell fluid. A 4 w/w% PEO in deionized water acted as the core fluid. These two liquids were fed at a constant flow rate independently controlled by two syringe pumps. To investigate the effect of the core flow rate on inner diameter of hollow PCL fibers, the typical flow rate for PCL solution was set at 3 mL h^{-1} or 6 mL h^{-1}. For PEO solutions, the flow rate was varied from 0.1 to 3.0 mL h^{-1}; to investigate the effect of the shell flow rate, the PEO flow rate was maintained at 0.4 mL h^{-1}, the PCL flow rate was changed in the range of 3 to 7 mL h^{-1}. Other co-ES parameters were as follows: electrostatic field of 1.8−2.0 kV cm^{-1}, working distance between the coaxial spinneret and the fiber collector of between 5 and 10 cm. The process was run for about 35 min to collect a 10-cm-long bundle of core−shell fibers.

Characterization of co-ES Fibers. The surface morphology and cross sections of co-ES fibers were observed using a Philips XL30 FEG SEM with an accelerating voltage of 5 kV. The co-ES fiber specimens were coated with a thin gold film to increase their conductivity. For imaging of the fiber cross sections, the fiber bundle was cut by sharp scissors in liquid nitrogen. Image processing software ImageJ (NIH) was used to measure the fiber inner diameters from the SEM micrographs. For each sample, fiber inner diameters were measured at 20 different points within SEM images to determine the average values and standard deviations. Co-ES fibers were also imaged by using an Olympus BH2-UMA optical microscope.

Phantom Preparation. Layers of electrospun fibers with 2 mL h^{-1} PEO core flow rate and 3 mL h^{-1} PCL shell flow rate (9 kV applied voltage, 5 cm working distance), were packed into 8 mm glass tubes, with the fibers aligned along the axis of the tubes. The tubes were filled with cyclohexane - a proton rich solvent capable of infusing into the hydrophobic polymer, with a suitable MRI properties to mimic the free liquid in axonal bodies (T_1 = 2328 ms and T_2 = 1329 ms at 22 °C and 1.5 T).[26]

MR Imaging. Diffusion tensor imaging using a pulsed gradient spin−echo with 30 gradient directions, b = 800 s mm^{-2} (plus 1 b = 0 s mm^{-2}), δ = 4 ms, Δ = 10 ms, G_{max} = 302.8 mT m^{-1} was carried out on a Bruker 7 T horizontal bore magnet (Bruker Biospin, Germany). Other sequence parameters were: axial FOV 2 cm × 2 cm, 128 × 128 matrix, total of 7 slices with 1 mm slice thickness, TR = 3.5 s, TE = 28.2 ms.

The MR signal comes from the cyclohexane that diffuses within the fibers. From the signal attenuation along the different directions the diffusion tensor was calculated; from this tensor the mean, parallel and

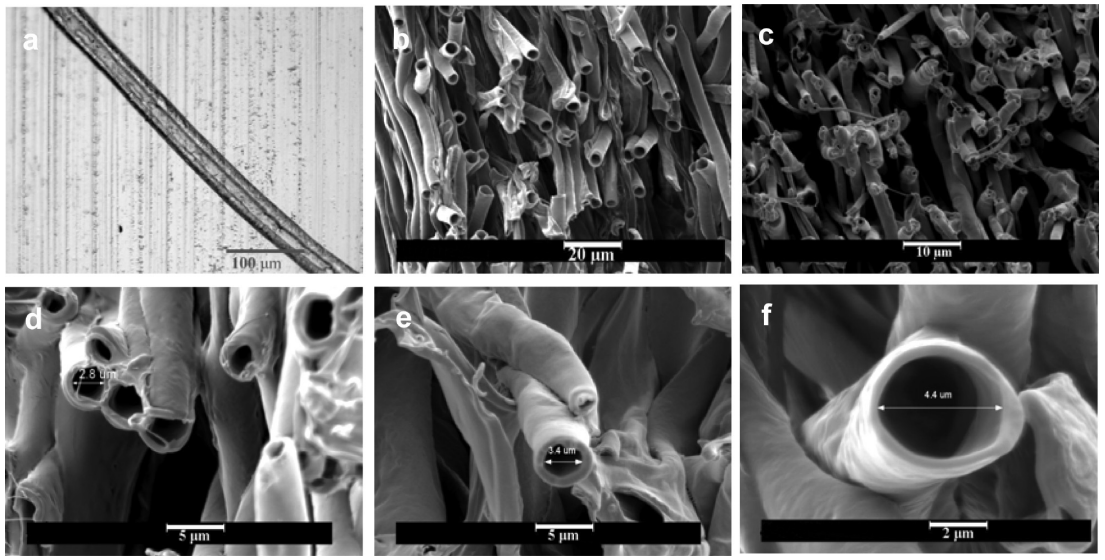

Figure 1. Optical microscopy image of (a) a PEO/PCL core/shell fiber; SEM images of cross sections of hollow PCL fibers using (b) PEO and (c) sugar core materials, and (d–f) hollow PCL fibers with various inner diameters using a PEO core material. Note: images b–f are not from the phantoms used for diffusion MR imaging, but are only to illustrate the formation of hollow fibers.

perpendicular diffusivities and fractional anisotropy were calculated.[27] The resultant images were masked to regions where mean diffusivity (MD) was lower than that recorded in the free cyclohexane, where $MD_{ch} = 1.4 \pm 0.07 \times 10^{-3}$ mm^2 s^{-1} at 22 °C. The mean and standard deviation of the MRI parameters were calculated within these regions of interest.

RESULTS AND DISCUSSION

Random PCL Hollow Fibers. PEO/PCL polymers were chosen as the core/shell materials to produce hollow fibers for the phantom preparation. Both PCL and PEO solutions can be electrospun as individual components, which resulted in a well-defined boundary between the core and the shell in the co-ES process of PEO/PCL, as seen from the optical microscopy image in Figure 1a. Figure 1b shows the cross section of PEO-PCL core–shell fibers randomly deposited on the collector plate. The cross sections of these coelectrospun fibers reveal that the resultant fibers are hollow and have much larger inner diameters than those from the sugar-PCL combination, as shown in Figure 1c. From these two core/shell solution pairs, PCL hollow fibers were fabricated in a one-step procedure by co-ES. The solvent evaporation in the core solutions is responsible for the formation of hollow fibers with uniform and strong walls by the co-ES process.[28] More importantly, a relatively wide range of core/shell flow rates allow a stable compound drop, Taylor cone and subsequent jet to be achieved in the co-ES of PEO/PCL core/shell solutions.[29] As an example of co-ES of PEO/PCL, we have shown that PCL hollow fibers with various inner diameters can be produced by adjusting the core flow rate in the co-ES process (Figures 1d-1f). Therefore, the PEO/PCL solution pair is an ideal choice for coaxial electrospinning to build up into a bulk PCL hollow fiber bundle, which is a requirement for the fabrication of phantom material suitable for dMRI.

Aligned Hollow PCL Fibers. It is well-known that, for a given polymer solution, the process stability during electrospinning can be significantly affected by two key process variables – the applied electric field and the flow rate. These variables have a certain range of values defined by operating diagrams, which have been used in electrospinning to demonstrate regions of different jet behaviors as a function of applied electric field and flow rate.[30−32] For a given core/shell solution pair in co-ES, the search for the operating diagrams is important for determining the appropriate values of the processing variables. For co-ES, however, it becomes more complicated because of combinational factors from the two different solutions.[33] In our previous study, extensive efforts were devoted to the exploration of the values of the electric field and core/shell flow rates in order to locate their operating diagrams, where a stable co-ES process could be achieved to produce an effective phantom material.[22] Within the operating diagrams, the core flow rate of PEO solution was adjusted to produce hollow PCL fibers with various inner diameters, while the PCL shell flow rate was maintained constant, since the inner diameter of hollow PCL fibers is expected to be one of key factors affecting the diffusion of the solvent in dMRI. SEM images shown in Figures 2a–h reveal the cross-sections of hollow PCL fibers produced at core flow rates varying from 0.1 to 2 mL h^{-1}, where the shell flow rate was maintained at 3 mL h^{-1}. As demonstrated in Figure 2i, the PCL fiber inner diameter increased from ∼3.3 to ∼10.2 μm as the core flow rate increased. A similar tendency was still observed for the effect of core flow rate when the shell flow rate was increased to 6 mL h^{-1} (Figure 2j). It can clearly be seen that the core flow rate has a significant impact on the inner diameter of co-ES hollow PCL fibers. The reproducibility of the inner diameters of the hollow PCL fibers was assessed using SEM images of eight samples produced using different core flow rates (images not shown here). As shown in Figure 2i, reproducibility is good.

Based on these results, the inner sizes of the PCL fibers can be readily adjusted to suit the application of axon-mimicking phantoms, by fine-tuning the core/shell flow rates. Compared with the effect of the core flow rate, no significant change was observed in the values of the inner diameter with an increase in shell flow rate, as evidenced by Figure 2k. This finding is in line with previous reports by Zussman et al.[29,34] However, it is worth mentioning that the range of shell flow rates used in this experiment had to be narrow in order to maintain the stability

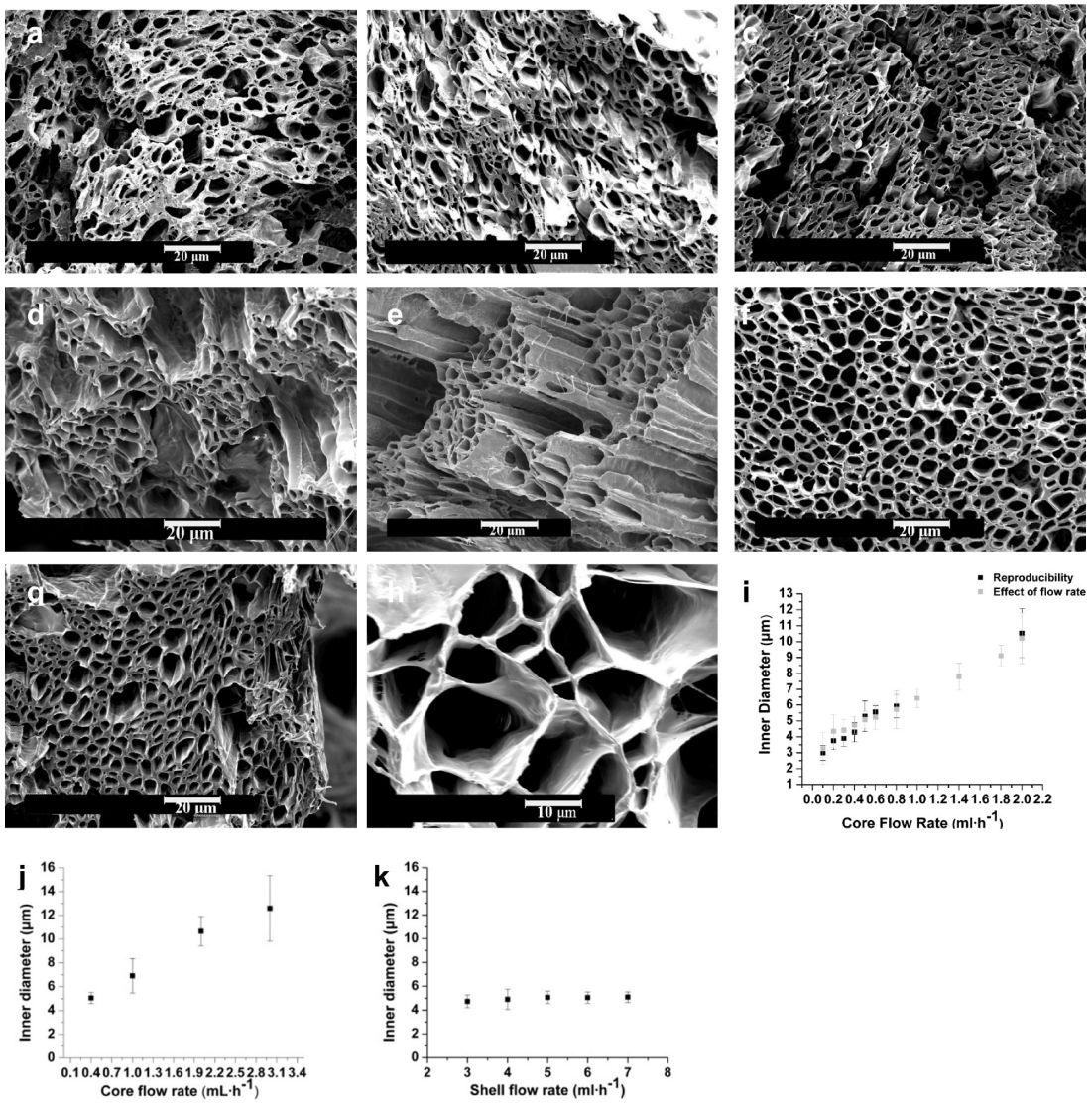

Figure 2. SEM images of hollow PCL fibers produced at different core flow rates: (a) 0.1, (b) 0.2, (c) 0.3, (d) 0.4, (e) 0.5, (f) 0.6, (g) 0.8, (h) 2 mL h^{-1}; (i) the relationship between the inner diameter of hollow PCL fibers and core flow rate at a 3 mL h^{-1} shell flow rate, showing good reproducibility; (j) the relationship between the inner diameter of hollow PCL fibers and PEO core flow rate at 6 mL h^{-1} shell flow rates, (k) the relationship between the inner diameter of hollow PCL fibers and shell flow rate. Experimental parameters: 9 kV applied voltage, 5 cm working distance, 3 mL h^{-1} PCL shell flow rate.

of the co-ES process, whereas the inner flow rate and electric field were fixed.

Stability of Hollow PCL Fibers. The design of physical phantoms requires careful consideration of suitable chemical stability.[35] The stability of electrospun hollow PCL fibers was assessed in cyclohexane, as this was to be used as a diffusion liquid for MR imaging. No obvious swelling or shrinking of co-ES fibers in the presence of cyclohexane over a 7 days period was observed (Figure 3a, b), even after its complete evaporation (Figure 3c). Images d and e in Figure 3 show this stability for the fiber bundle in cyclohexane.

MR Imaging. The details of the phantom construction for diffusion MRI can be found in the experimental section. Figure 4a shows the fibers packed in a glass tube, containing the solvent. In dMRI, it is the molecular diffusion of these solvent molecules to which the signal is sensitive. Any restriction or hindrance to the free diffusive passage of these solvent molecules leads to a change in the resultant MRI signal. By measuring the apparent diffusion coefficient in multiple directions, it is possible to elucidate the orientation of these barriers. In an anisotropic system, such as the hollow aligned fibers studied here, the greatest free diffusion (or highest diffusion coefficient) will be observed parallel to the fiber alignment. Figure 4b shows a colormap of the direction of the highest free/least restricted diffusion and, therefore, the principal direction of the fibers in the bundles. According to the color key ball in the figure, fibers running into and out of the page appear red, from left to right appear green, and up and down appear blue. The figure clearly shows the principal direction of the aligned fibers to be along the axis of the tube, as anticipated from the construction of the phantom.

Figure 4c shows the mean diffusivity (MD) of the solvent for the fibers; the average value is $0.45 \pm 0.28 \times 10^{-3}$ mm^2 s^{-1}. The average parallel diffusivity is $0.68 \pm 0.27 \times 10^{-3}$ mm^2 s^{-1} and the perpendicular diffusivity is $0.33 \pm 0.29 \times 10^{-3}$ mm^2 s^{-1}, compared with $1.4 \pm 0.07 \times 10^{-3}$ mm^2 s^{-1} for free cyclohexane. Figure 4d shows the fractional anisotropy (FA); the average value is 0.52 ± 0.22. Compared with the average MD and FA

dx.doi.org/10.1021/am301919s | ACS Appl. Mater. Interfaces 2012, 4, 6311−6316

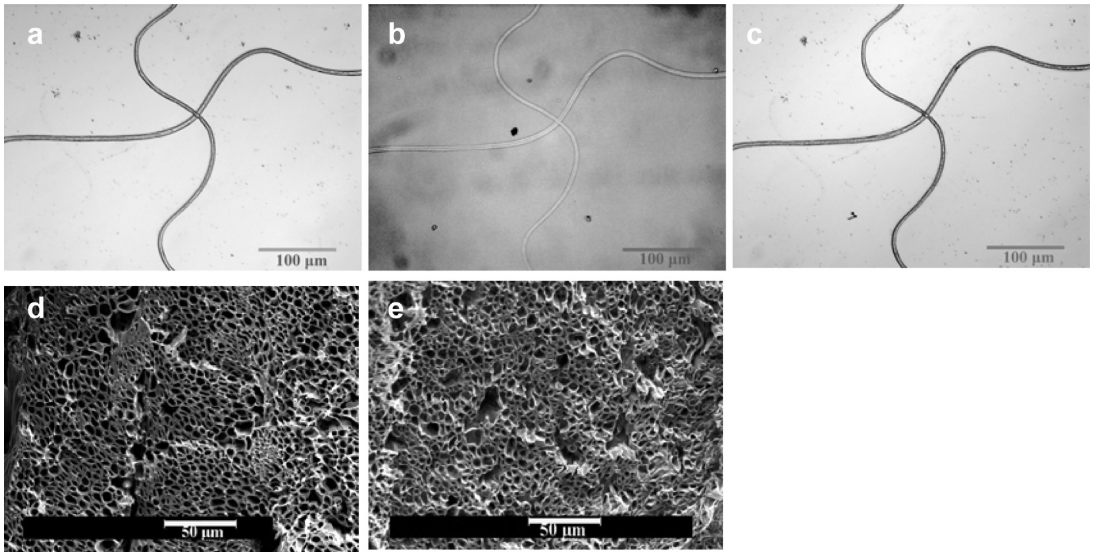

Figure 3. Optical microscope images of (a) as-spun hollow PCL fibers, (b) wet PCL fibers in cyclohexane after 7 days, (c) dried PCL fibers; SEM images of (d) as-spun hollow PCL fibers, (e) hollow PCL fibers after 7 days in cyclohexane.

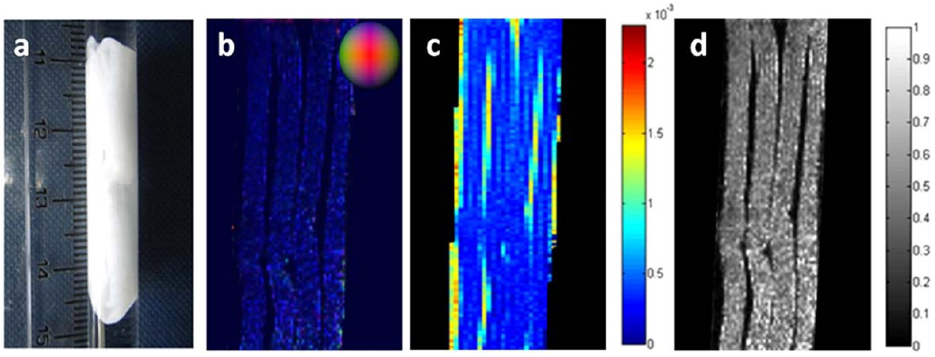

Figure 4. (a) Photograph of hollow PCL fiber phantoms in a glass tube filled with solvent. (b) RGB colormap of single slice through the phantom, revealing the consistent preferential alignment of the micrometer-scale fiber along the axis of the tube (i.e., blue, according to the color sphere key). (c) A mean diffusivity map (units 1×10^{-3} mm^2 s^{-1}) of the phantom, revealing lower values in the phantom compared with the free solvent (MD_{ch} = $1.4 \pm 0.07 \times 10^{-3}$ mm^2 s^{-1}). (d) A fractional anisotropy map showing that diffusion within the phantom is anisotropic (approaching 1) and in the solvent is isotropic (approaching 0).

values observed the ex vivo optic nerve of a rat by Richardson et al[10] (MD = $0.148 \pm 0.01 \times 10^{-3}$ mm^2 s^{-1}; FA = 0.86 ± 0.02), our MD value is higher and our FA value lower. Our values are, however, in the approximate in vivo biological range for white matter.[27] If we consider that the average diameter of the fibers in the phantom is 10.2 ± 1.6 μm, which is consistent with large axons in white matter,[18] we may expect our MD value to be a little higher and our FA value a little lower than in the optic nerve. These ex vivo MD and FA values are however respectively lower and higher than what is generally observed in tissue in vivo. The phantom sample temperature in our experiments is however 15 °C lower than body temperature (used in the Richardson study), suggesting that factors such as the use of cyclohexane as a solvent and the relative lack of microstructural complexity in the phantom when compared with biological tissue may also play an important role in the parameter value differences. In future work, we plan to study the effects of changing the inner diameter of the fibers on the diffusion signal, of adding an "extracellular" space to the phantom, and of increasing the structural complexity and biomimicry by adding inclusions to the "intra-cellular" space and by patterning the fibers.

CONCLUSIONS

To summarize, we have demonstrated that a novel brain white matter mimicking phantom comprising of aligned co-ES hollow polymeric fibers can be constructed and used to acquire diffusion magnetic resonance images. The inner diameter of co-ES hollow fibers was tuned by controlling the core flow rate and core/shell solution pairs in order to provide structures with similar inner diameters to axon fibers in brain white matter. We have shown that an anisotropic co-ES hollow fiber phantom is a stable test object that may be suitable for use as a quantitative validation and calibration tool for dMRI. The results of our study provide preliminary evidence that this phantom can mimic the cellular barriers imposed by axonal cell membranes and myelin. We have demonstrated that the measured diffusivity is within the range of the brain's white matter.[27] Work is underway in our laboratory to optimize co-ES fibers in terms of alignment, packing density and intricate geometries. Research in this area has the potential to enable the development of co-ES biomimetic phantoms that can mimic a range of biological structures within the body, potentially providing substitutes for animal tissues, and allowing the stable

and reproducible validation and calibration of diffusion MRI in a number of organs.

AUTHOR INFORMATION

Corresponding Author

*E-mail: geoff.parker@manchester.ac.uk.

Notes

The authors declare no competing financial interest.

ACKNOWLEDGMENTS

The project "CONNECT" acknowledges the financial support of the Future and Emerging Technologies (FET) Programme within the Seventh Framework Programme for Research of the European Commission, under FET-Open Grant 238292.

REFERENCES

(1) Parker, G. J. M. In *Diffusion MRI*; Jones, D. K., Ed.; Oxford University Press: Oxford, U.K., 2011; pp 396−408.

(2) Behrens, T. E. J.; Jbabdi, S. In *Diffusion MRI*; Johansen-Berg, H.; Behrens, T. E. J., Eds.; Academic Press: Amsterdam, 2009; pp 333−351.

(3) Assaf, Y.; Cohen, Y. In *Diffusion MRI*; Johansen-Berg, H., Behrens, T. E. J., Eds.; Academic Press: Amsterdam, 2009; pp 127−146.

(4) Hubbard, P. L. Parker, G. J. M. In *Diffusion MRI*; Johansen-Berg, H.; Behrens, T. E. J., Eds.; Academic Press: Amsterdam, 2009; pp 353−375.

(5) Boujraf, S. D.; Luypaert, R.; Eisendrath, H.; Osteaux, M. *Magn. Reson. Mater Phys.* **2001**, *13*, 82−90.

(6) Assaf, Y.; Freidlin, R. Z.; Rohde, G. K.; Basser, P. J. *Magn. Reson. Med.* **2004**, *52*, 965−978.

(7) Descoteaux, M.; Angelino, E.; Fitzgibbons, S.; Deriche, R. *Magn. Reson. Med.* **2006**, *56*, 395−410.

(8) Pullens, P.; Roebroeck, A.; Goebel, R. *J. Magn. Reson. Imaging* **2010**, *32*, 482−488.

(9) Fieremans, E.; Deene, Y. D.; Delputte, S.; Odemir, M. S.; D'Asseler, Y.; Vlassenbroeck, J.; Deblaere, K.; Achten, E.; Lemahieu, I. J. *Magn. Reson.* **2008**, *190*, 189−199.

(10) Richardson, S.; Siow, B.; Batchelor, A. M.; Lythgoe, M. F.; Alexander, D. C. *Magn. Reson. Med.* **2012**, DOI: 10.1002/mrm.24410.

(11) Fieremans, E.; Deene, Y. D.; Delputte, S.; Ozdemir, M. S.; Achten, E.; Lemahieu, I. *Phys. Med. Biol.* **2008**, *53*, 5405−5419.

(12) Poupon, C.; Rieul, B.; Kezele, I.; Perrin, M.; Poupon, F.; Mangin, J. F. *Magn. Reson. Med.* **2008**, *60*, 1276−1283.

(13) Perrin, M.; Poupon, C.; Cointepas, Y.; Rieul, B.; Golestani, N.; Pallier, C.; Riviere, D.; Constantinesco, A.; Le Bihan, D.; Mangin, J. F. *IPMI Proc.* **2005**, *3565*, 52−63.

(14) Fillard, P.; Descoteaux, M.; Goh, A.; Gouttard, S.; Jeurissen, B.; Malcolm, J.; Ramirez-Manzanares, A.; Reisert, M.; Sakaie, K.; Tensaouti, F.; Yo, T.; Mangin, J. F.; Poupon, C. *NeuroImage* **2011**, *56*, 220−234.

(15) Gates, L.; Cameront, I. *Proc. ISMRM* **1998**, 1259.

(16) Anderson, J. R.; Ackerman, J. J. H.; Carbow, J. R. *Concepts Magn. Reson. B* **2011**, *39B*, 149−158.

(17) Anderson, J. R.; Ye, Q.; Niel, J. J.; Ackerman, J. J. H.; Garbow, J. R. *J. Magn. Reson.* **2011**, *211*, 30−36.

(18) Perge, J. A.; Niven, J. E.; Mugnaini, E.; Balasubramanian, V.; Sterling, P. J. *Neuroscience* **2012**, *32*, 626−638.

(19) Histology of the Heart (n.d.), Retrieved May 2, 2012, from http://www.courseweb.uottawa.ca/medicine-histology/english/cardiovascular/histologyheart.htm.

(20) Agarwal, S.; Wendorff, J. H.; Greiner, A. *Adv. Mater.* **2009**, *21*, 3343−3351.

(21) Grafahrend, D.; Heffels, K.-H.; Beer, M. V.; Gasteier, P.; Moller, M.; Boehm, G.; Dalton, P. D.; Groll, J. *Nat. Mater.* **2011**, *10*, 67−73.

(22) Zhou, F. -L.; Hubbard, P. L.; Eichhorn, S. J.; Parker, G. J. M. *Polymer* **2011**, *52*, 3603−3610.

(23) Zhou, F.-L.; Gong, R. H.; Porat, I. *Polym. Int.* **2009**, *58*, 331−342.

(24) Kang, Y. K.; Park, C. H.; Kim, J.; Kang, T. J. *Fiber Polym.* **2007**, *8*, 564−570.

(25) Kim, G. H.; Son, J. G.; Park, S. A.; Kim, W. D. *Macromol. Rapid Commun.* **2008**, *29*, 1577−1581.

(26) Tofts, P. S.; Lloyd, D.; Clark, C. A.; Barker, G. J.; Parker, G. J. M.; McConville, P.; Baldock, C.; Pope, J. M. *Magn. Reson. Med.* **2000**, *43*, 368−374.

(27) Jones, D. K. *Cortex* **2008**, *44*, 936−952.

(28) Dror, Y.; Salalha, W.; Avrahami, R.; Zussman, E.; Yarin, A. L.; Dersch, R.; Greiner, A.; Wendorff, J. H. *Small* **2007**, *3*, 1064−1073.

(29) Arinstein, A.; Avrahami, R.; Zussman, E. *J. Phys. D: Appl. Phys.* **2009**, *42*, 015507.

(30) Shin, Y. M.; Hohman, M. M.; Brenner, M. P.; Rutledge, G. C. *Polymer* **2001**, *42*, 09955−09967.

(31) Hohman, M. M.; Shin, M.; Rutledge, G. C.; Brenner, M. P. *Phys. Fluids* **2001**, *13*, 2221−2240.

(32) Wang, C.; Hsu, C. H.; Hwang, I. H. *Polymer* **2008**, *49*, 4188−4195.

(33) Moghe, A. K.; Gupta, B. S. *Polym. Rev.* **2008**, *48*, 353−377.

(34) Reznik, S. N.; Yarin, A. L.; Zussman, E.; Bercovici, L. *Phys. Fluids* **2006**, *18*, 1−13.

(35) Kwan, R. K.-S.; Evans, A. C.; Pike, G. B. *IEEE Trans. Med. Imaging* **1999**, *18*, 1085−1097.